A CGCM Study on the Interaction between IOD and ENSO

SWADHIN K. BEHERA, JING JIA LUO, SEBASTIEN MASSON, SURYACHANDRA A. RAO, AND HIROFUMI SAKUMA

Frontier Research Center for Global Change/JAMSTEC, Yokohama, Japan

TOSHIO YAMAGATA*

Department of Earth and Planetary Science, University of Tokyo, Tokyo, Japan

(Manuscript received 19 July 2005, in final form 29 November 2005)

ABSTRACT

An atmosphere–ocean coupled general circulation model known as the Scale Interaction Experiment Frontier version 1 (SINTEX-F1) model is used to understand the intrinsic variability of the Indian Ocean dipole (IOD). In addition to a globally coupled control experiment, a Pacific decoupled noENSO experiment has been conducted. In the latter, the El Niño–Southern Oscillation (ENSO) variability is suppressed by decoupling the tropical Pacific Ocean from the atmosphere. The ocean–atmosphere conditions related to the IOD are realistically simulated by both experiments including the characteristic east–west dipole in SST anomalies. This demonstrates that the dipole mode in the Indian Ocean is mainly determined by intrinsic processes within the basin. In the EOF analysis of SST anomalies from the noENSO experiment, the IOD takes the dominant seat instead of the basinwide monopole mode. Even the coupled feedback among anomalies of upper-ocean heat content, SST, wind, and Walker circulation over the Indian Ocean is reproduced.

As in the observation, IOD peaks in boreal fall for both model experiments. In the absence of ENSO variability the interannual IOD variability is dominantly biennial. The ENSO variability is found to affect the periodicity, strength, and formation processes of the IOD in years of co-occurrences. The amplitudes of SST anomalies in the western pole of co-occurring IODs are aided by dynamical and thermodynamical modifications related to the ENSO-induced wind variability. Anomalous latent heat flux and vertical heat convergence associated with the modified Walker circulation contribute to the alteration of western anomalies. It is found that 42% of IOD events affected by changes in the Walker circulation are related to the tropical Pacific variabilities including ENSO. The formation is delayed until boreal summer for those IODs, which otherwise form in boreal spring as in the noENSO experiment.

1. Introduction

The Indian Ocean dipole (IOD) is identified as one of the leading modes of climate variabilities in the Tropics. A positive IOD event starts from an anomalous cooling near the Java coast in response to the intensified southeasterly trade winds in boreal spring. It then manifests as a basinwide dipole mode marked by opposite anomalies, particularly in sea surface temperature (SST) on either side of the tropical Indian Ocean. The positive IOD grows through the coupled feedback among anomalies of SST, upper-ocean heat content, wind, and precipitation (e.g., the review article by Yamagata et al. 2004), similar to the cold episode of El Niño–Southern Oscillation (ENSO; Bjerknes 1969). During its peak phase in boreal fall, IOD rigorously affects rainfall over East Africa and Indonesia (e.g., Saji et al. 1999; Behera et al. 2005) in addition to several other regions of the globe (Saji and Yamagata 2003).

It is observed that several significant IOD events have occurred in the absence of ENSO events; the correlation between the dipole mode index (DMI) and the Niño-3 (5°N–5°S, 150°–90°W) SST index is 0.34 (Saji et al. 1999). However, in a seasonally stratified analysis

* Additional affiliation: Frontier Research Center for Global Change/JAMSTEC, Yokohama, Japan.

Corresponding author address: Dr. Swadhin Behera, Frontier Research Center for Global Change/JAMSTEC, Showa-machi, Yokohama, Kanagawa 236-0001, Japan.
E-mail: behera@jamstec.go.jp

the DMI–Niño-3 correlation increases to 0.56 during boreal fall. Although this is not a necessary condition for dependency of two phenomena, a few studies questioned the independence of IOD from ENSO (e.g., Hastenrath 2002; Baquero-Bernal et al. 2002). The independent nature of some of the IOD events is not hard to trace; simple composites of SST anomalies derived from pure IOD events that are not associated with ENSO events illustrate the existence of the basin-wide dipole pattern (cf. Yamagata et al. 2004). Therefore, it is unlikely that the IOD is an ENSO-forced mode though there is a likelihood of interaction between them in concurrent years. Hence, for predictability studies, it is necessary to evaluate first the intrinsic characteristics of IOD and ENSO and then to clarify possible interactions between them. For this purpose, we use an atmosphere–ocean coupled general circulation model (CGCM) known as the Scale Interaction Experiment Frontier version 1 (SINTEX-F1) model. Realistic simulation results of IOD and ENSO by the SINTEX-F1 (Yamagata et al. 2004; Behera et al. 2005; Tozuka et al. 2005, 2006) encourage us to employ the model in regional decoupling experiments. We will see later that the SINTEX-F1 model provides a useful means to understand the independent features of the IOD and its modification owing to the interaction with ENSO.

The IOD variability is also discussed in several other CGCM studies (Iizuka et al. 2000; Baquero-Bernal et al. 2002; Gualdi et al. 2003; Lau and Nath 2004; Yu and Lau 2004; Ashok et al. 2004; Wajsowicz 2005; Cai et al. 2005). Most of them captured both IOD and ENSO events in their model study with a certain amount of covariability. While Iizuka et al. (2000) reported a weak relation between IOD and ENSO in their model study, Baquero-Bernal et al. (2002) could not find a coupled mode in the Indian Ocean in the absence of ENSO. Yu and Lau (2004) also reported that IOD is primarily ENSO-forced besides the Indian monsoon that operated in absence of ENSO.

In this study, we have performed a couple of numerical experiments using the SINTEX-F1 CGCM to separate coupled variabilities in the Indian and Pacific Oceans. In one of the experiments, IOD variability is separated from the ENSO variability by decoupling the tropical Pacific as in Behera et al. (2005). Comparison between results from this model experiment and that from a globally coupled control experiment shows that the IOD is essentially an intrinsic ocean–atmosphere coupled mode of the Indian Ocean. In contrast to the finding of Baquero-Bernal et al. (2002), it is found that the major features of the subsurface variabilities in the Indian Ocean are preserved in the absence of ENSO. It is difficult to compare our results fully with previous CGCM studies under inadequate information on model biases. Nevertheless, in the following sections we try to capture some aspects qualitatively using our analyses and observational results on the possible relation between IOD and ENSO.

2. Model and data

The SINTEX-F1 adapted to run on the Earth Simulator is an upgraded version (see Luo et al. 2003; Masson et al. 2005) of the SINTEX model described in Gualdi et al. (2003). In the present version, the atmospheric component ECHAM-4 (Roeckner et al. 1996) is fully coupled to the ocean component Ocean Parallélisé (OPA8.2; Madec et al. 1998) through the Ocean–Atmosphere–Sea Ice–Soil (OASIS 2.4; Valcke et al. 2000) coupler. The atmosphere model has a spectral representation in the horizontal with a triangular truncation at wavenumber 106 (T106) and has 19 discrete vertical levels. This spectral resolution is roughly equivalent to a horizontal grid mesh of $1^\circ \times 1^\circ$. The ocean model OPA8.2 using the ORCA2 grid adopts the Arakawa C grid with a finite mesh of $2^\circ \times 0.5^\circ$ cosine(latitude); the meridional grid resolution increases toward the equator with a grid length of 0.5° in the equatorial region. To avoid the singularity in the coordinate system, the finite mesh is designed in a way that the North Pole is replaced by two nodal points located over North America and Eurasia. The model has 31 levels in the vertical. The details of the coupling strategy are reported in Guilyardi et al. (2001). As in SINTEX (e.g., Gualdi et al. 2003), the SINTEX-F1 has shown remarkable skill in reproducing variabilities in the Indian and Pacific Oceans (Luo et al. 2003, 2005a,b; Yamagata et al. 2004; Masson et al. 2005; Behera et al. 2005; Tozuka et al. 2005; Tozuka et al. 2006; Rao et al. 2005, manuscript submitted to *J. Climate*, hereafter RAO). The monthly data from the last 200 yr of the total 220-yr model results are used in the present analysis.

In addition to the 220-yr-long control experiment, we performed an additional model experiment to suppress ENSO variability by decoupling the tropical Pacific. The decoupling strategy is similar to what is reported in Behera et al. (2005). In the decoupling procedure climatological SSTs between 25°N and 25°S, instead of evolving interannual SSTs, derived from the last 200-yr result of the control experiment are supplied to the atmospheric model as the lower boundary condition. This effectively suppresses the ENSO evolution in the coupled model while allowing the independent evolution of IOD. The 70-yr decoupled experiment is named the noENSO experiment.

Observed SST anomalies are computed from the Hadley Centre Sea Ice and SST (HadISST1.1) dataset (Rayner et al. 2003), and heat content (from surface to 125 m) anomalies are derived from the simple ocean data assimilation (SODA) products (Carton et al. 2000) for the period 1958–2001. Following Saji et al. (1999), the DMI is defined as the SST anomaly difference between the western (10°S–10°N, 50°–70°E) and eastern (10°S–0°, 90°–110°E) tropical Indian Ocean. The western box (10°S–10°N, 40°–60°E) of model DMI is slightly westward of that in observed data. This is because anomalies near the eastern pole in the model are seen to spread far more into the central Indian Ocean as compared to observations. The zonal wind index (ZWI) is derived as in Saji et al. (1999) from the area average over the domain 5°S–5°N, 70°–90°E for both model and observed data. The Niño-3 index is derived from the HadISST1.1 data averaged for the region 5°N–5°S, 150°–90°W.

Simple linear statistical tools such as composite and correlation methods are used in the analyses. IOD years are identified when the eastern pole and western pole are in opposite phase and DMI exceeds 1σ in September–November. Statistical significance of the correlation coefficients is determined by a two-tailed Student's t test. To focus on interannual variations, low-frequency variations of periodicity longer than 7 yr are removed from all the datasets with a high-pass Butterworth filter.

3. Dominant modes of interannual variability

Before discussing modes of interannual variability, we briefly describe a few important features of the Indian Ocean climatology from SINTEX-F1 results. In general, seasonal characteristic of SST, thermocline, wind, and rainfall in the Indian Ocean (cf. Hastenrath et al. 1993) are captured well by the SINTEX-F1 simulation (see Behera et al. 2005). Similar seasonal variabilities also are found in the noENSO experiment results. The southeasterlies in boreal summer cross the equator and turn into southwesterlies on the western Indian Ocean. As a result of these winds, the thermocline is shallow in the west compared to that in the east where the warm pool is prominent (Fig. 1). Nevertheless, the thermocline rises in the east during boreal fall when the seasonal southeasterly trade winds cross the equator in the east, which is prominent in the non-ENSO experiment results (Fig. 1c). These seasonal conditions of the eastern Indian Ocean introduce the seasonal phase-locking characteristic of the IOD; the equatorial westerlies reverse to easterlies along with the rise in seasonal thermocline in the east during a positive IOD event.

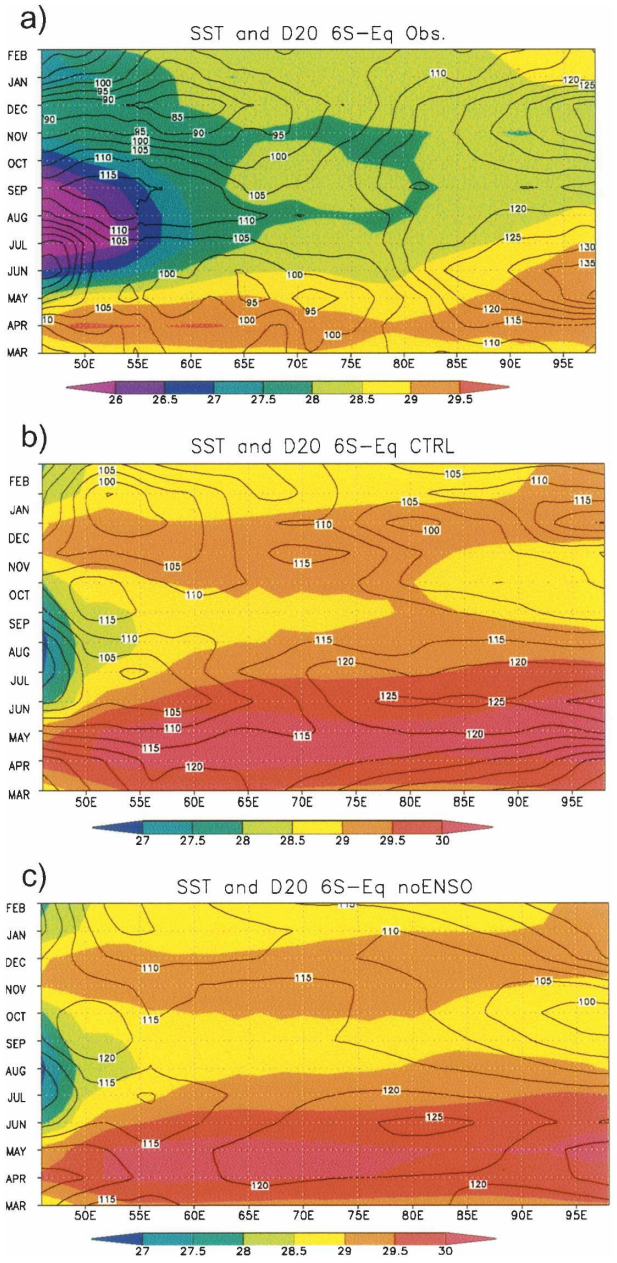

FIG. 1. Longitude–time section averaged between 6°S and the equator for climatological (a) SST (shaded) derived from the HadISST data and depth of 20°C (contoured) derived from SODA. (b) Same as in (a), but for model SST and depth of 20°C in the control experiment. (c) Same as in (b), but for the noENSO experiment. SST unit is °C and depth of 20°C unit is m.

The SST variability in the tropical Indian Ocean is also influenced by changes in surface heat fluxes in response to variabilities in clouds and surface winds. Generally evaporative cooling and solar insolation compete with ocean dynamics to determine SST evolution in the western and southern Indian Ocean (e.g., Behera et al.

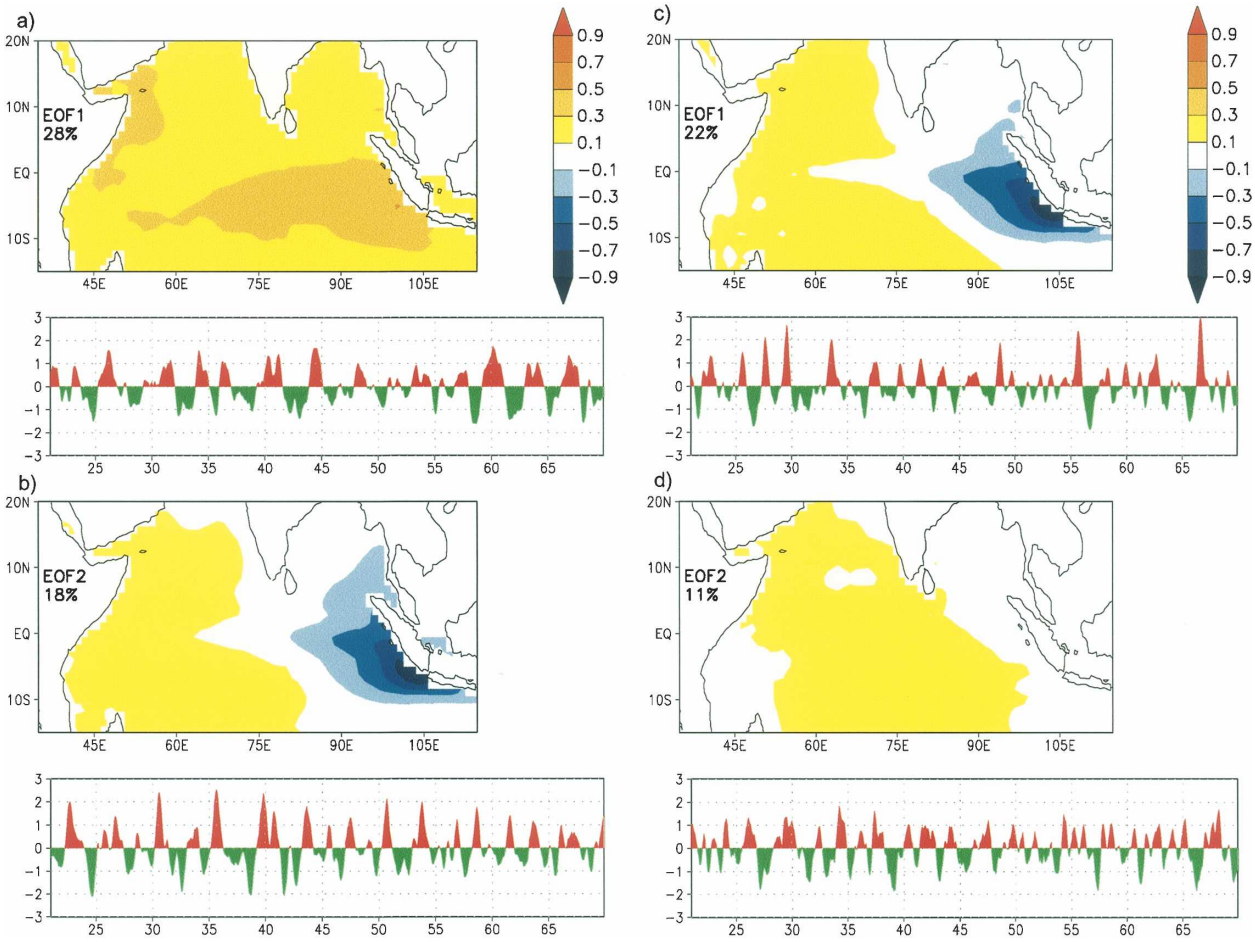

FIG. 2. (a), (b) First and second EOF modes along with their principal components for surface temperature anomalies derived from control experiment results. (c), (d) The corresponding first and second EOF modes along with their principal components for noENSO experiment results.

2000). The seasonal cycle in the heat flux is shown to be influenced by interannual climate anomalies such as ENSO. The ENSO influence on the SST anomalies of the Indian Ocean is manifested as a basinwide pattern of uniform polarity. Typically, the tropical Indian Ocean warms (cools) in response to a warm (cold) ENSO event from concurrent boreal winter to next boreal spring (see, e.g., Pan and Oort 1990; Kawamura 1994; Tourre and White 1995; Klein et al. 1999; Venzke et al. 2000; Huang and Kinter 2002). This is captured as the first EOF mode in SST anomalies (e.g., Yamagata et al. 2004), which is also simulated well by the model (Fig. 2a). In contrast to this basinwide single polarity pattern, the second EOF mode of the Indian Ocean SST anomalies is a dipole with opposite loadings on either side of the basin. The dipole pattern of the second EOF (Fig. 2b) is comparable to that in the observation (e.g., Fig. 1b of Yamagata et al. 2004); the IOD appears as a major interannual coupled mode during many of the model years in the SINTEX-F1 simulation (Yamagata et al. 2004; Behera et al. 2005). But, less frequent occurrences of this mode compared to the first EOF mode lowers IOD to the second dominant seat in the EOF analysis.

This less prominent seat in EOF analyses sometimes leads to the misunderstanding that the dipole mode is an artifact of the statistical analyses. Several studies argued that an inverse relation as in IOD anomalies does not exist between the east and the west (Dommenget and Latif 2002; Baquero-Bernal et al. 2002; Hastenrath 2002). It is now understood that this interpretation is not always correct (Yamagata et al. 2003; Behera et al. 2003). Since the basinwide uniform mode dominates the SST variability on an interannual time scale, we need to filter out the externally forced mode to find the signal related to IOD in a linear statistical analysis. As shown in Yamagata et al. (2003), a remarkable seesaw is found between the east and the west

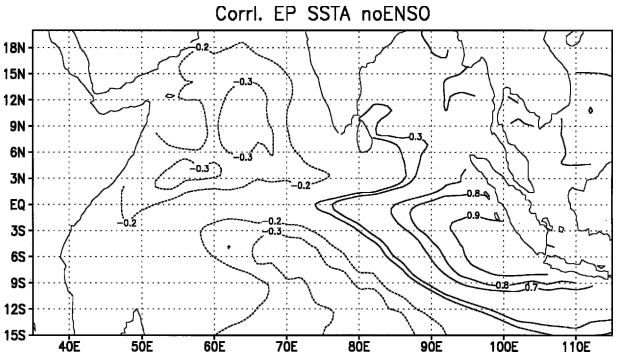

FIG. 3. Correlation of the eastern pole of the IOD with the basinwide SST anomalies from noENSO experiment results. Shown correlation coefficients exceed the 99% confidence level from a two-tailed Student's *t* test.

after removing the ENSO-related variability (readers are referred to Fig. 3 of their article), and the dipole mode takes a dominant seat in the EOF decomposition after removing the ENSO-related first EOF mode (Behera et al. 2003). It remains to be seen how much of this linear statistical partition is realistic in an ocean–atmosphere coupled environment as underscored in the model results of Baquero-Bernal et al. (2002). The non-ENSO model experiment provides an opportunity for this verification.

Proving the previous statistical analyses true, the dipole mode appears as the first EOF mode (Fig. 2c) in the noENSO SST anomalies. Moreover, a negative correlation pattern emerges in the western Indian Ocean from the correlation between the eastern pole and the basinwide SST anomalies (Fig. 3). Therefore, this model experiment confirms that the IOD variability takes the dominant seat in absence of the ENSO variability, which induces a dominant monopole mode in the Indian Ocean. It is also noted that the present finding does not agree with the previous findings of Baquero-Bernal et al. (2002) and Yu and Lau (2004). Based on their model experiments, those two studies suggest that IODs are primarily ENSO forced. In particular, Baquero-Bernal et al. (2002) suggest that the dipole mode, which is only detected during boreal fall in their CGCM results, is not necessarily related to the ocean dynamics and is rather forced stochastically by the atmosphere. From the analysis of SINTEX-F1 model results, we confirm the independent nature of IOD and its possible interaction with ENSO. We have basically shown examples of positive IOD events. The processes related to the negative IOD events are essentially opposite to those in positive IOD events unless otherwise stated.

4. Intrinsic variability of IOD and interaction with ENSO

a. Frequency

One of the key features of IOD is the strong correlation between the SST anomalies and the zonal wind anomalies in the central equatorial region (Saji et al. 1999; Rao et al. 2002; Yamagata et al. 2003, 2004; Behera et al. 2003, 2005). This intrinsic ocean–atmosphere coupling is shown in Fig. 4. The ZWI in boreal fall is significantly correlated to the anomalies of SST and heat content (from surface to 300 m). The correlations

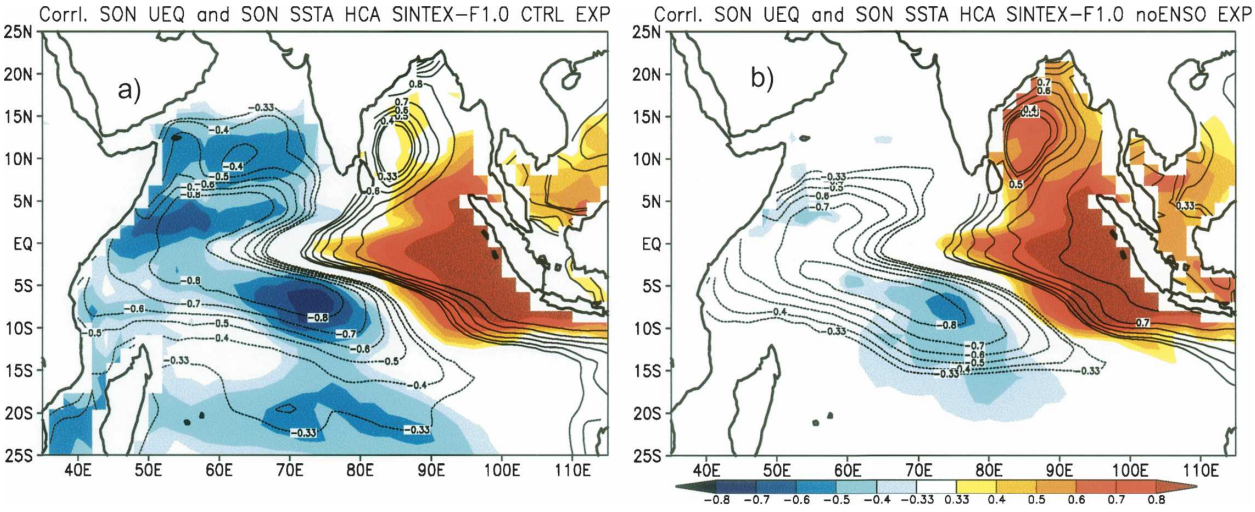

FIG. 4. September–November concurrent correlation of ZWI with SST anomalies (shaded) and the heat content anomalies (contour) for the tropical Indian Ocean in the (a) control experiment and (b) noENSO experiment. Shown correlation coefficients exceed the 99% confidence level from a two-tailed Student's *t* test.

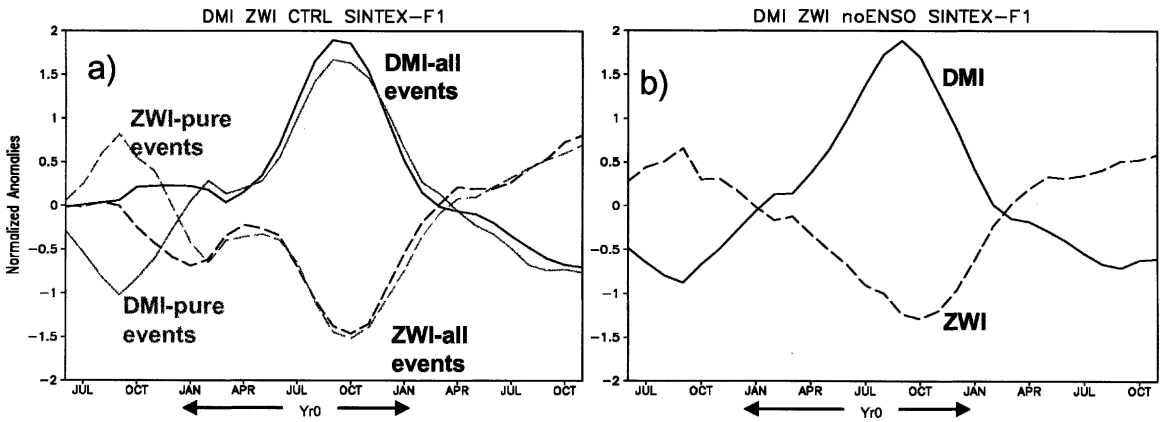

FIG. 5. Composites [(positive − negative)/2] of coevolving DMI and ZWI for the (a) control experiment and (b) noENSO experiment from a year before to a year after a strong positive IOD year. Both indices are normalized by respective standard deviations. Composites of pure IOD events from the control experiment are shown in light gray. The concurrent year is shown as Yr0 in the abscissa. Shown values exceed 90% of confidence limit from a two-tailed Student's *t* test.

between the ZWI and anomalies of SST and heat content are already significant in June–August one season prior to the peak IOD season. This ocean–atmosphere coupling related to the IOD as found in observations and the control experiment (e.g., Yamagata et al. 2004) is also resolved well in the noENSO experiment. In contrast to the finding of Baquero-Bernal et al. (2002), we find from the ZWI–heat content correlation that the subsurface Indian Ocean plays a significant role in the IOD development in absence of ENSO variability. It is quite likely that the results of Baquero-Bernal et al. (2002) are either influenced by model biases or a misrepresentation of the dipole mode when their atmospheric model is coupled to a mixed layer ocean model. In that model experiment the major center of action appears to be in the subtropical Indian Ocean. We note that the subtropical region in the Indian Ocean is basically driven by atmospheric forcings, sometimes giving rise to a subtropical dipole mode (e.g., Behera and Yamgata 2001; Suzuki et al. 2004a). It is possible that the subtropical dipole contaminated the model results of Baquero-Bernal et al. (2002).

Similar to observation, the ZWI and DMI evolve in March–April, peak in September–October, and decay by January–February in the noENSO experiment results (Fig. 5). In addition, as seen in the observations (e.g., Fig. 3 in Saji et al. 1999), negative events pave the way for positive IOD events in the noENSO experiment (Fig. 5b) as well as pure positive IOD events of the control experiment (Fig. 5a). However, composites of all IOD events in the control experiment are biased by several concurrent IOD and ENSO events. In most of the following discussions, we refer to these events as concurrent IOD events. It is found that the ENSO modifies some of the IOD characteristics during these concurrent events. In results of both experiments the positive IOD events typically turn to subsequent negative events and vice versa. Though this tendency is not apparent in Fig. 3 of Saji et al. (1999), Rao et al. (2002) report such a tendency in recent decades and provide a detailed characteristic path of ocean waves that elucidate the phase reversal of the IOD. Prominence of this cyclic (negative–positive–negative) nature of IOD events gives rise to a remarkable biennial tendency in the wavelet spectrum of DMI in the noENSO experiment (Fig. 6a). The spectrum in the biennial band is weak in the control experiment as well as in the observation. Instead we find a prominent spectral peak at the 3–4-yr band in the control experiment, which is closer to the spectral peak at the 4–6-yr band in the observed data (Fig. 6a). In addition, we have shown spectra of the eastern and western poles of the IOD separately in Figs. 6c and 6d. For the noENSO experiment, the spectra of both poles (as discussed in section 2) show enhanced variability for periods of about 2 yr as compared to those of control experiment results. This further confirms the existence of the independent biennial IOD in contrast to the finding of Baquero-Bernal et al. (2002). It is the tropical Pacific influence that is mainly responsible for the sluggish nature of the interannual IOD variability, which is intrinsically quasi biennial. This interesting aspect has been recently studied from a viewpoint of the heat budget in the tropical Indian Ocean by Tozuka et al. (2006).

Interestingly, we find a spectral peak at 3–4 yr in the Niño-3 index of control experiment results (Fig. 6b). In another sensitivity experiment where the ocean and atmosphere are decoupled in the tropical Indian Ocean (noIOD experiment), the ENSO periodicity is protracted to a 5–6-yr spectral peak. This aspect of the

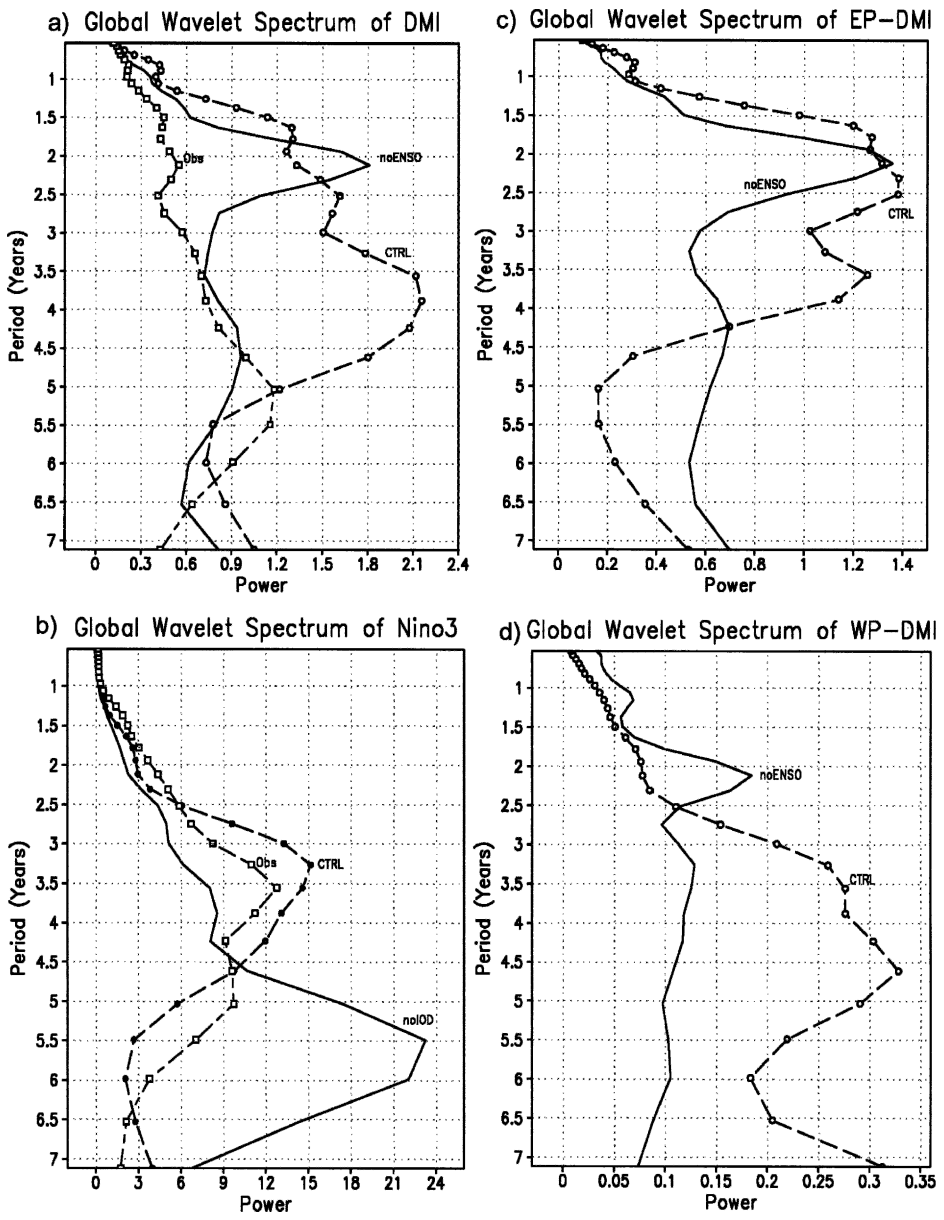

FIG. 6. (a) Global wavelet spectrum of the DMI derived from the noENSO experiment (solid line), control experiment (dashed lines marked by circles), and observation (dashed line marked by squares). (b) Same as in (a), but for Niño-3 index except for the solid line, which is for the noIOD experiment. (c), (d) The wavelet spectra for the noENSO experiment (solid line) and control experiment (dashed lines marked by circles) for the eastern pole and the western pole, respectively.

IOD influence on ENSO will be reported in the second part of this study. These model experiments show that the frequency modulation of IOD and ENSO to a great extent is determined by their interaction. In the absence of such an interaction, the basin size and land–sea distribution perhaps decide their intrinsic periodicity. In the following we discuss the mechanism that determines the biennial tendency in IOD variability. This is also true for independent IOD variability in the control experiment. It is found that the presence of ENSO and other coupled variabilities in the tropical Pacific disrupt the natural choice of biennial variability of IOD. This is discussed in section 4c.

The role of subsurface ocean on the surface variability in the western Indian Ocean has been discussed in several previous studies (e.g., Murtugudde and Busallachi 1999; Webster et al. 1999; Behera et al. 2000; Rao et al. 2002; Xie et al. 2002; Feng and Meyers 2003; Shinoda

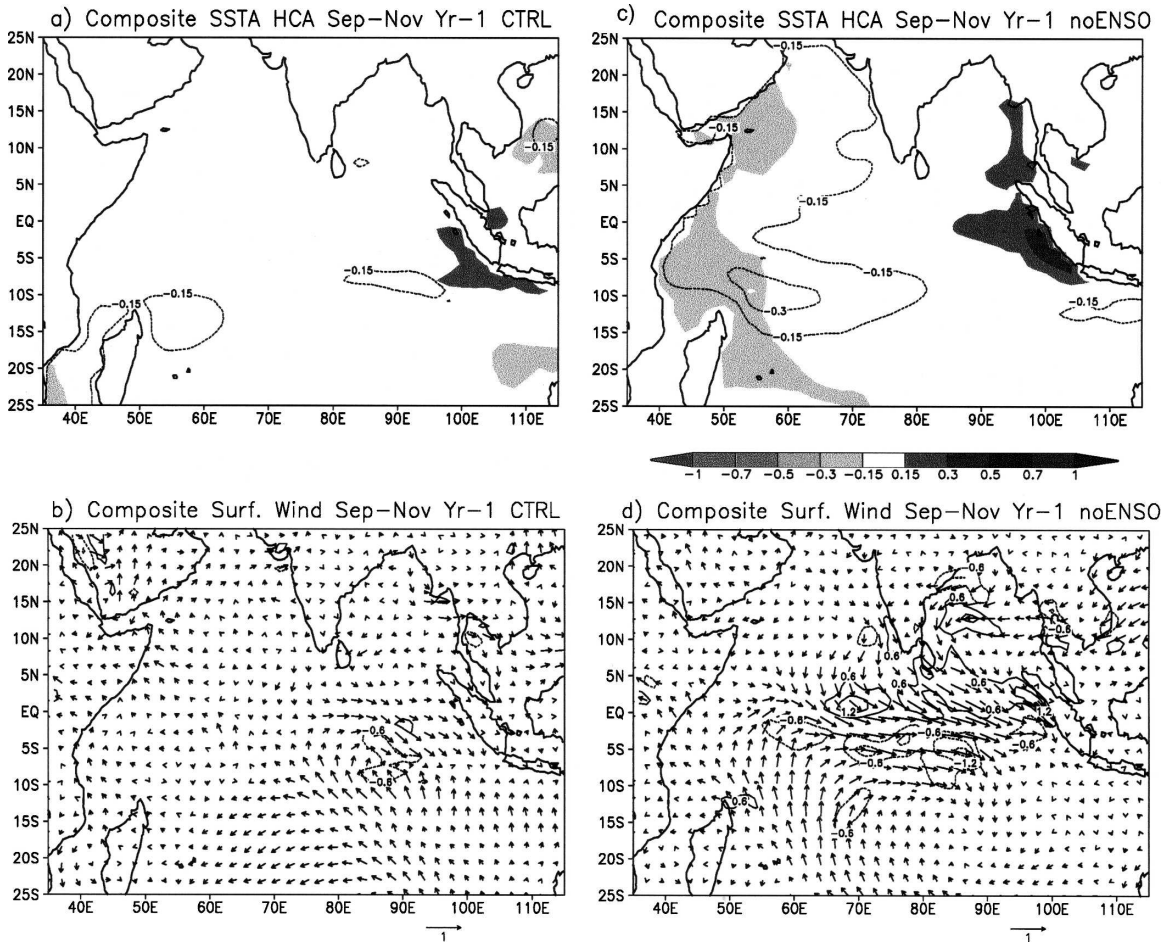

FIG. 7. September–November composites [(positive − negative)/2] for anomalies of SST shown in shading and heat content (W) shown in contour computed for a year before a significant IOD event in the (a) control experiment and (c) noENSO experiment. The corresponding composites for anomalies of wind (m s^{-1}) and wind stress curl (N m^{-3}) are shown for the (b) control experiment and (d) noENSO experiment. All shown values exceed 90% of confidence limit from a two-tailed Student's *t* test. Heat content anomalies (in contour) are scaled by a factor of 10^9 and wind stress curl anomalies are multiplied by a factor of 10^9.

et al. 2004; Yamagata et al. 2004; Rao and Behera 2005; Jury and Huang 2004; Suzuki et al. 2004b; Tozuka et al. 2006). In particular, using a 2.5-layer reduced gravity model (McCreary et al. 1993), Behera et al. (2000) suggested that the ocean dynamics around 5°S in southwestern Indian Ocean determine the SST variability throughout the year. Moreover, studies of Yamagata et al. (2004) and Rao and Behera (2005) show that interannual oceanic Rossby waves associated with the IOD in the equatorial Indian Ocean influence the SST in the southwestern Indian Ocean. Here we notice that the composite plots of the anomalies of heat content and SST show the presence of weak negative IOD events in boreal fall of one year before positive IOD events (Fig. 7) in the case of the noENSO experiment. Such anomalies in heat content and wind are not evident in the control experiment since composites are biased by concurrent IODs (Figs. 7a,b). In the noENSO experiment, the anomalous westerlies (Fig. 7d) associated with these negative events favor upwelling in the western Indian Ocean (Fig. 7c). As a result of those upwelling-favorable winds we find negative heat content and cold SST anomalies in the western side of the basin. In the subsequent months, these negative heat content anomalies propagate westward and then reach the equator as coastal Kelvin waves. Thereafter, those heat content anomalies propagate to the Sumatra–Java coast as equatorial Kelvin waves. The anomalous rise in the thermocline and associated SST cooling there in March–April (Fig. 8) then trigger a positive IOD event. In a similar way a signal from the Arabian Sea also propagates to the Sumatra coast to trigger the IOD as found by Suzuki et al. (2004b). A negative IOD event develops in an opposite manner. As discussed here, anomalous

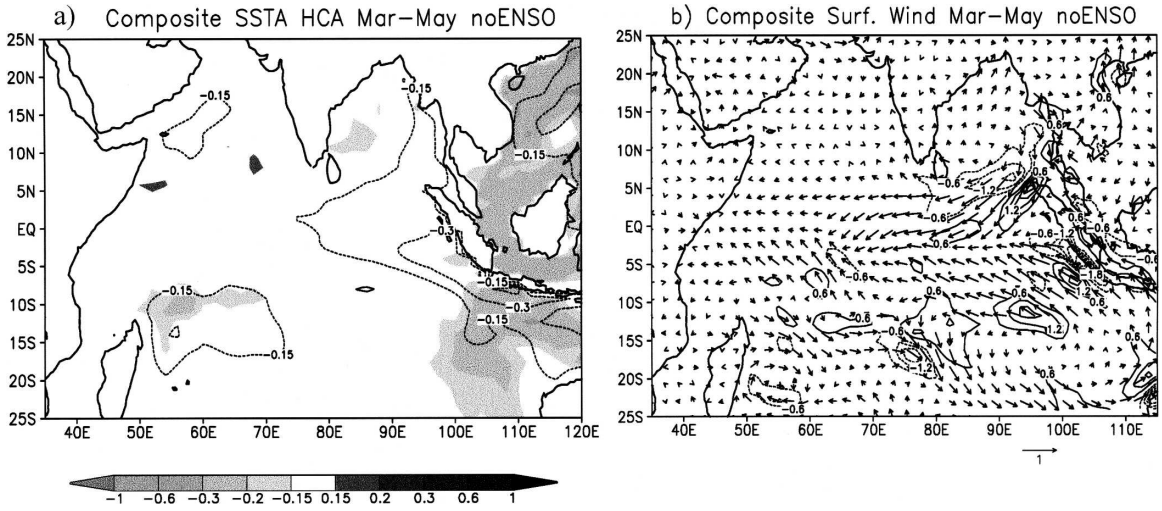

FIG. 8. (a) Same as in Fig. 7c, but for the composites corresponding to March–May of the IOD year in the noENSO experiment and (b) the corresponding composites for wind and wind stress curl.

monsoon winds play an important role in the equatorial southwestern Indian Ocean to modulate the biennial IOD events in the noENSO experiment. Interestingly, it is found that those anomalous monsoon winds in the southern tropical Indian Ocean are not necessarily related to the Indian monsoon variability in our model results: The correlation between the Indian summer monsoon rainfall[1] and the DMI is not significant, either for concurrent seasons or for 1-yr lead–lag seasons, in both noENSO and control experiment results. Therefore, it is unlikely that the Indian monsoon affects the periodicity of the IOD though the positive IODs sometimes evolve together with the above-normal Indian monsoon conditions. In the control experiment, the Indian Ocean variability not only relates to changes in monsoon winds in the southern tropical Indian Ocean but also the Indonesian Throughflow and meridional heat transport as discussed in Tozuka et al. (2006). The latter two processes sometimes are influenced by ENSO events via oceanic and atmospheric connections to disrupt the biennial variability of the IOD. This is discussed in section 4c.

In addition to the seasonal variability, intraseasonal disturbances (ISDs) play an important role in the IOD evolution. The wind anomalies associated with ISDs trigger downwelling equatorial Kelvin waves that upon reaching the eastern coasts suppress the thermocline there to terminate a positive IOD event (Rao and Yamagata 2004; RAO). In the discussions above, it is found that cold anomalies prevailed in the western Indian Ocean before the development of a positive IOD event. From the analyses of 20–40 days of wind anomalies as in RAO, we notice that the cold western Indian Ocean substantially reduces the ISD activity between December and May in the noENSO experiment; no ISD activities are detected in 90% of positive IOD cases, and only weak events are found in the rest. On the contrary, warm anomalies in the west prior to a negative IOD event favor ISD activity, thereby helping the formation of a negative IOD event. ISD activities are detected for all negative IOD events during May–June that coincide the occurrence of the spring Yoshida–Wyrtki jet in the equatorial Indian Ocean. It is observed that the spring jet plays a significant role in the IOD development (Vinayachandran et al. 1999; Suzuki et al. 2004b). In the absence of significant cold/warm precondition in the western Indian Ocean, sporadic ISD activities unsettle several IOD evolutions in the control experiment (e.g., Rao and Yamagata 2004).

b. Amplitude

Here we discuss how the amplitude of IOD is influenced by ENSO. Composites of the anomalies of SST and heat content are shown in Fig. 9 for the peak IOD season from September to November. It is found that the SST anomalies tend to be weaker in the southwestern equatorial Indian Ocean for the western pole of IOD in the noENSO experiment (Fig. 9c) as compared to that in the control experiment (Fig. 9a). This is consistent with the finding of Yu and Lau (2004) that the western anomalies are somewhat stronger in concur-

[1] Rainfall anomalies averaged over the region (10°–30°N, 70°–95°E) for the June–September season.

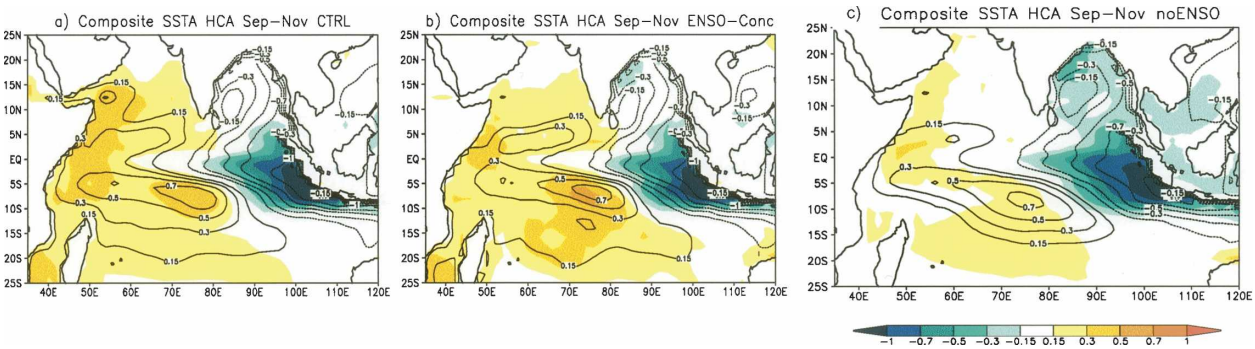

FIG. 9. Same as in Fig. 7a, but for the September–November composites in the (a) control experiment, (b) IOD events concurrent with ENSO events in the control experiment, and (c) noENSO experiment.

rent IOD events. Here, we find that the difference in the anomalies of the western box, between the noENSO experiment and the control experiment, is also apparent in the heat content anomalies and heat flux anomalies. So, it is possible that the ocean dynamics and surface heat fluxes contribute to stronger SST anomalies in the western pole for concurrent IODs. This possibility is examined by preparing composites of SST anomalies for concurrent IOD events (Fig. 9b). Since there is not much difference found between Fig. 9a and Fig. 9b, it is expected that the composite for the SST anomalies in the control experiment (Fig. 9a) is biased by concurrent IOD events (Fig. 9b). Contrary to the composites of concurrent IODs, the composites of noENSO experiments resemble that of the pure IOD events extracted from the control experiment (cf. Yamagata et al. 2004) and observed data (Fig. 10b). Possible causes of the additional western warming in concurrent positive IOD events are explored by analyzing atmospheric and oceanic connections between the two basins.

The contemporaneous ENSO influence on IOD can be realized by both the atmospheric Walker cell and the Indonesian Throughflow (e.g., Tozuka et al. 2006). The latter process is apparent by the slight reduction in the heat content anomalies in the western Indian Ocean for the noENSO experiment (Fig. 9). Though the Rossby wave phase speed remains unchanged in both model experiments, the amplitude of the downwelling Rossby waves in the western part is stronger in the concurrent

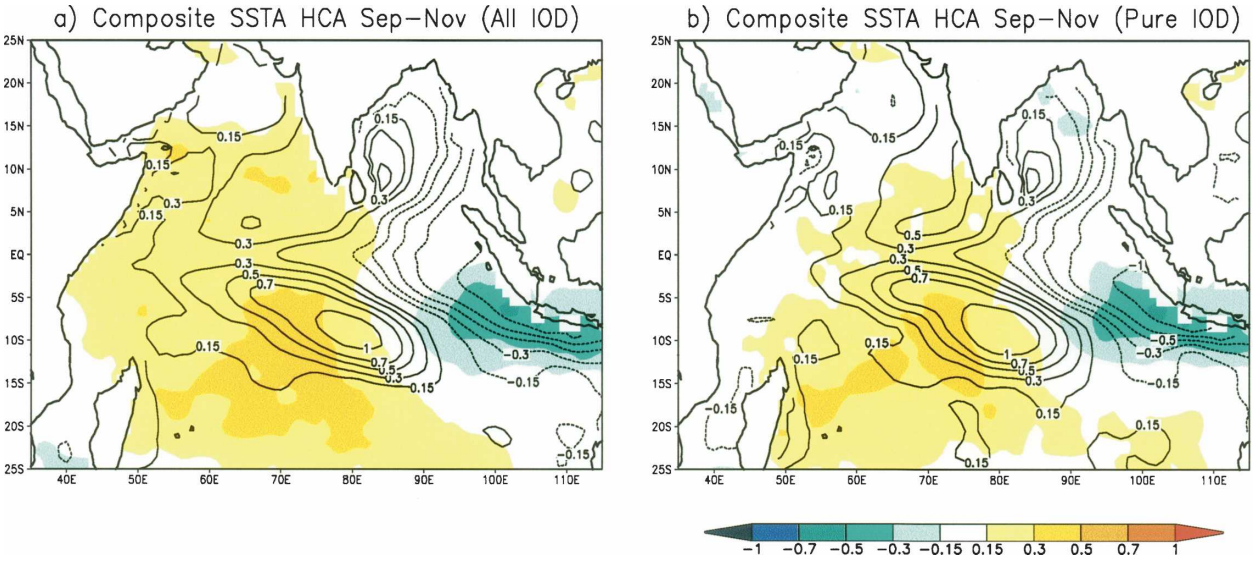

FIG. 10. Same as in Fig. 9a, but for anomalies of SST and heat content (°C m) derived from HadISST data and SODA, respectively, in cases of (a) all IOD events and (b) pure IOD events. Years for all and pure IOD events are adapted from Yamagata et al. (2004). Heat content anomalies are scaled by a factor of 200.

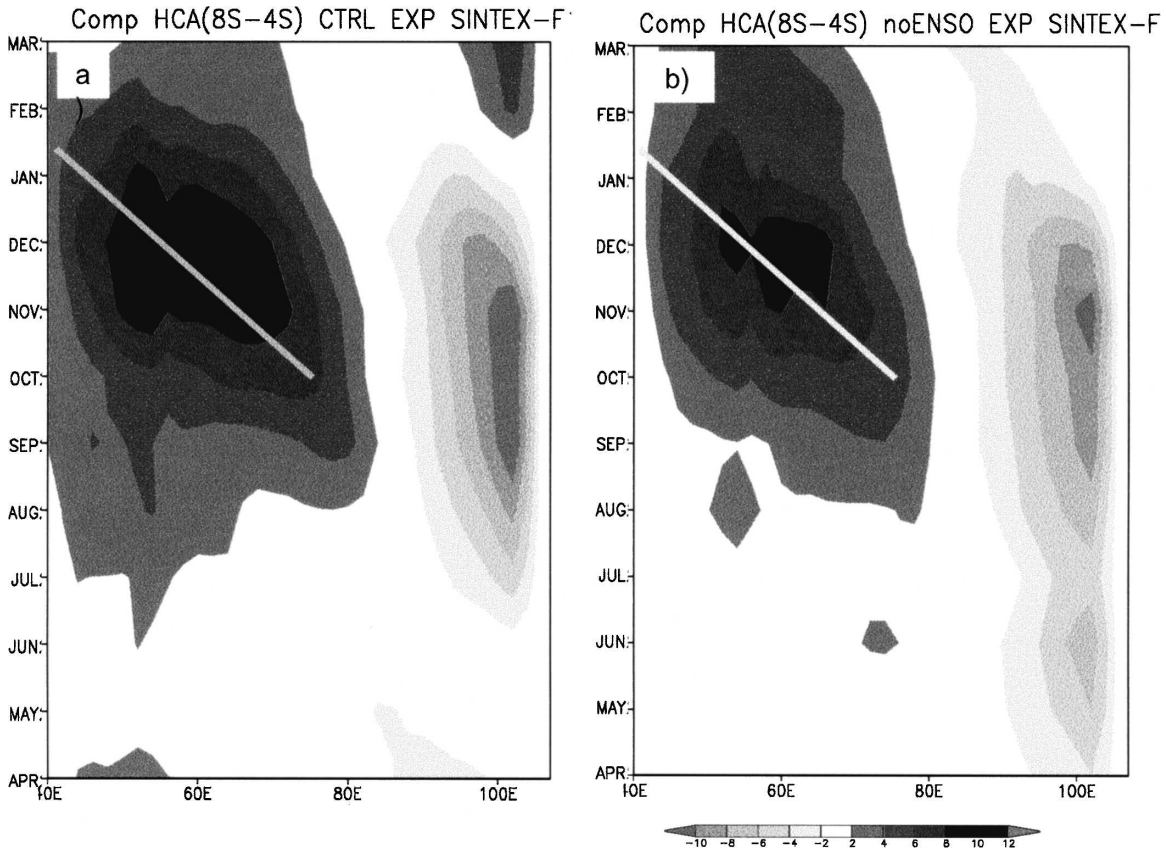

FIG. 11. Longitude–time sections of composites of model heat content anomalies (W) averaged between 8° and 4°S in the case of the (a) control experiment and (b) noENSO experiment. Anomalies are scaled by a factor of 10^9. Shown values exceed the 90% level of statistical significance from a two-tailed Student's *t* test.

IODs (Fig. 11). Therefore, ocean dynamics play a role in deciding the strength of western warming. Another possibility is that coevolving ENSOs influence the SST anomalies in the western pole of the concurrent IODs through changes in heat fluxes associated with the Indo-Pacific Walker circulation. Figure 12 shows the seasonal composites of velocity potentials from boreal summer to fall. In the control experiment, the upper (lower)-tropospheric convergence (divergence) covers most parts of the tropical Indian Ocean during boreal summer (Fig. 12a) of positive IOD events. On the contrary, in the noENSO experiment upper (lower)-tropospheric divergence (convergence) appears over the western part (Fig. 12c) in response to the Indian Ocean anomalous Walker cell that is already established in summer. Thus, surface winds (from the center of low-level divergence to the other center of low-level convergence) tend to be stronger in the western part for IODs in the noENSO experiment as compared to those of concurrent IODs. In the latter case, the western warming for positive IODs (Fig. 13b) is seen during boreal summer aided by weaker evaporative cooling (Fig. 13a) and stronger vertical heat convergence in the upper ocean. In the noENSO experiment, stronger evaporation (Fig. 13c) and weaker vertical heat convergence reduce the anomalous western warming (Fig. 13d).

The Walker cell in the Indian Ocean intensifies (Figs. 12b,d) during the peak season of the IOD with upper (lower)-tropospheric divergence (convergence) in the west and opposite conditions in the east. However, lower-tropospheric convergence is stronger for the noENSO IODs as compared to that for the concurrent IODs. This suggests that stronger winds related to the lower-tropospheric convergence in the west lead to higher evaporative loss and colder SST in the noENSO IODs. Though the SST anomalies in some parts of the western pole tend to be weaker in the case of the noENSO experiment, as found from model results and data, it did not affect the short rains variability much in the neighboring East Africa (Behera et al. 2005). This is because the moisture convergence to East Africa remains unaffected.

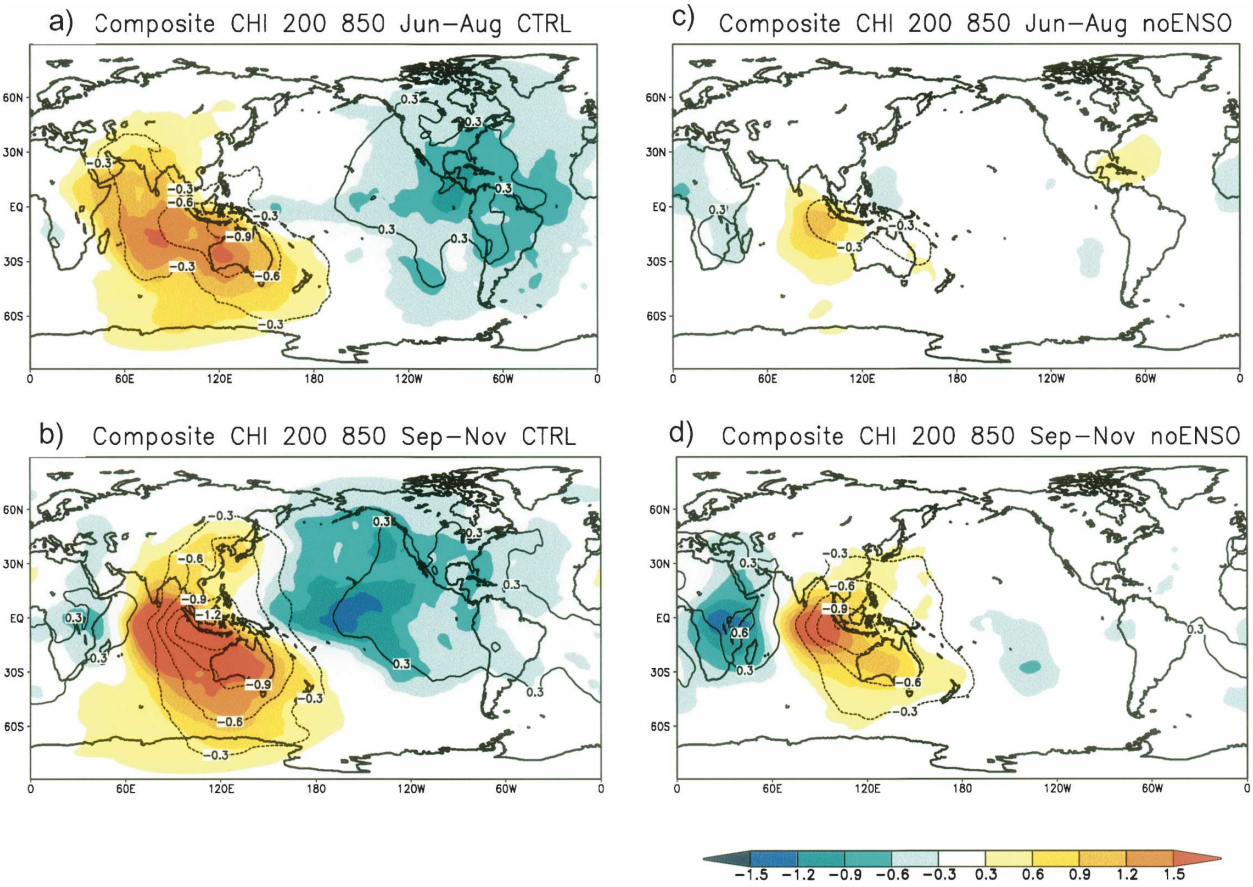

FIG. 12. Composites of velocity potential anomalies ($m^2 s^{-1}$) for (a) June–August of control experiment results, (b) September–November of control experiment results, (c) June–August of noENSO experiment results, and (d) September–November of noENSO experiment results. Anomalies are scaled by a factor of 10^6. Anomalies from 200 (850) hPa are shaded (contoured). Shown values exceed the 90% level of statistical significance from a two-tailed Student's *t* test.

c. Formation

Several mechanisms are proposed to explain the formation of IOD. One important mechanism that favors IOD formation is the development of an anomalous high over the eastern Indian Ocean (e.g., Saji et al. 1999; Behera et al. 1999; Gualdi et al. 2003; Li et al. 2003; Annamalai et al. 2003). Based on data analyses, Behera and Yamagata (2003) show that the sea level pressure anomalies in the eastern Indian Ocean are related to the local SST changes. As discussed in previous subsections, significant anomalies in heat content and SST are already seen in the eastern Indian Ocean in boreal spring prior to an IOD event though less apparent in control experiment results. Here, we find significant lagged correlations between the boreal fall ZWI and the boreal spring global sea level pressure anomalies (Fig. 14). The correlation patterns are mostly seen over the southern Indian Ocean. From analyses of the SINTEX coupled model results, Gualdi et al. (2003) suggested that the anomalous high in the southeastern Indian Ocean is significantly correlated to the sea surface temperature anomalies of the tropical Indian and Pacific Oceans. It is also found from observed data that the equatorial winds in the Indian Ocean are related to variabilities in pressure and trade winds of the southern Indian Ocean (Hastenrath and Polzin 2004). As discussed in section 4a, consequent to intrinsic ocean dynamics, cold anomalies from the western Indian Ocean prior to a positive IOD reach the Sumatra–Java coast during boreal spring (Fig. 8a) in the noENSO experiment. Associated with these cold anomalies, the suppressed convection induces the anomalous high over the southeastern Indian Ocean. This favors equatorial easterly anomalies off Sumatra–Java and alongshore winds that trigger a positive IOD through an atmosphere–ocean feedback process. Since the process is pronounced in the noENSO case, it is no wonder that

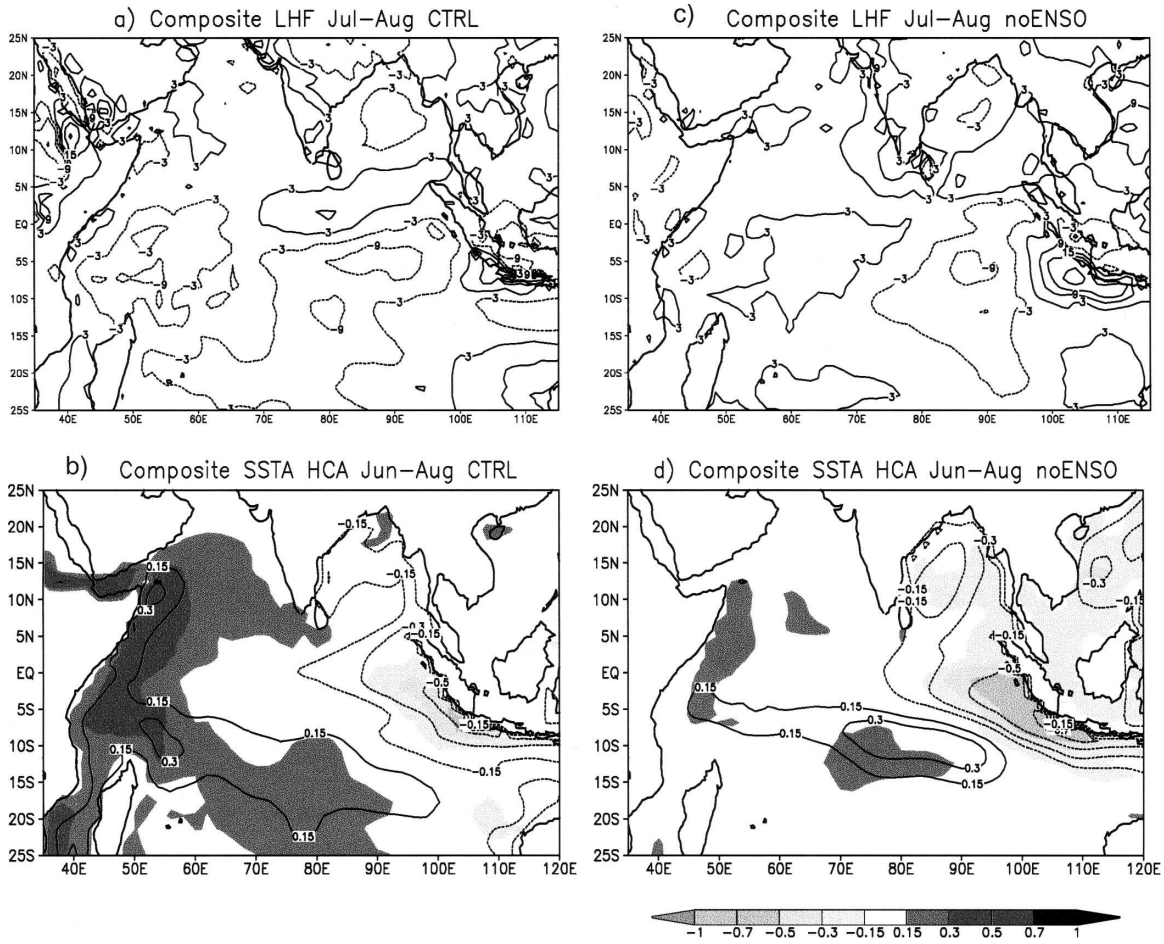

FIG. 13. June–August composites of latent heat flux anomalies (W m^{-2}) for the (a) control experiment and (c) noENSO experiment. Corresponding composites for (b) SST (°C) and (d) heat content (W) anomalies. Negative latent heat flux anomalies indicate heat gain by the ocean. Heat content anomalies are scaled by a factor of 10^9. Values shown exceed the 90% level of statistical significance from a two-tailed Student's *t* test.

84% (83%) of positive (negative) IOD events develop from favorable equatorial wind anomalies[2] associated with the anomalous high and the local SST changes. The results from the noENSO experiment suggest that the remote forcing from Pacific SST anomalies is not essential for the IOD formation even if they might affect the IOD formation in concurrent IOD years.

The remote influence of the Pacific SST anomalies on the IOD formation is apparent in the control experiment. We find 58% (56%) of positive (negative) IOD events develop from a favorable condition of the equatorial zonal wind anomaly. It is found in the remaining 42% (44%) of positive (negative) events that a favorable condition is significantly introduced at a later stage by the presence of coupled variability in the tropical Pacific. This leads to reduction in the IOD predictability based on those early symptoms of equatorial winds in the Indian Ocean. It also raises an interesting question: how does the remaining 42% (44%) of positive (negative) IOD events evolve in spite of the unfavorable condition in boreal spring? The process is essentially opposite in reverse cases where positive (negative) IOD cannot develop in spite of a favorable condition.

In Fig. 15, we have shown the composites of velocity potential anomalies related to years when unfavorable conditions in boreal spring turned to favorable ones in

[2] The boreal spring zonal wind anomalies are considered favorable (unfavorable) when in-phase (out of phase) ZWI exceeds 0.25σ in March–May in the years of IOD. Negative (positive) ZWI is considered to be in phase (out of phase) with positive IOD and vice versa for negative IOD. As stated in section 2, IOD years are identified based on the criteria that the eastern pole and western pole are in opposite phase and DMI exceeds 1σ in September–November.

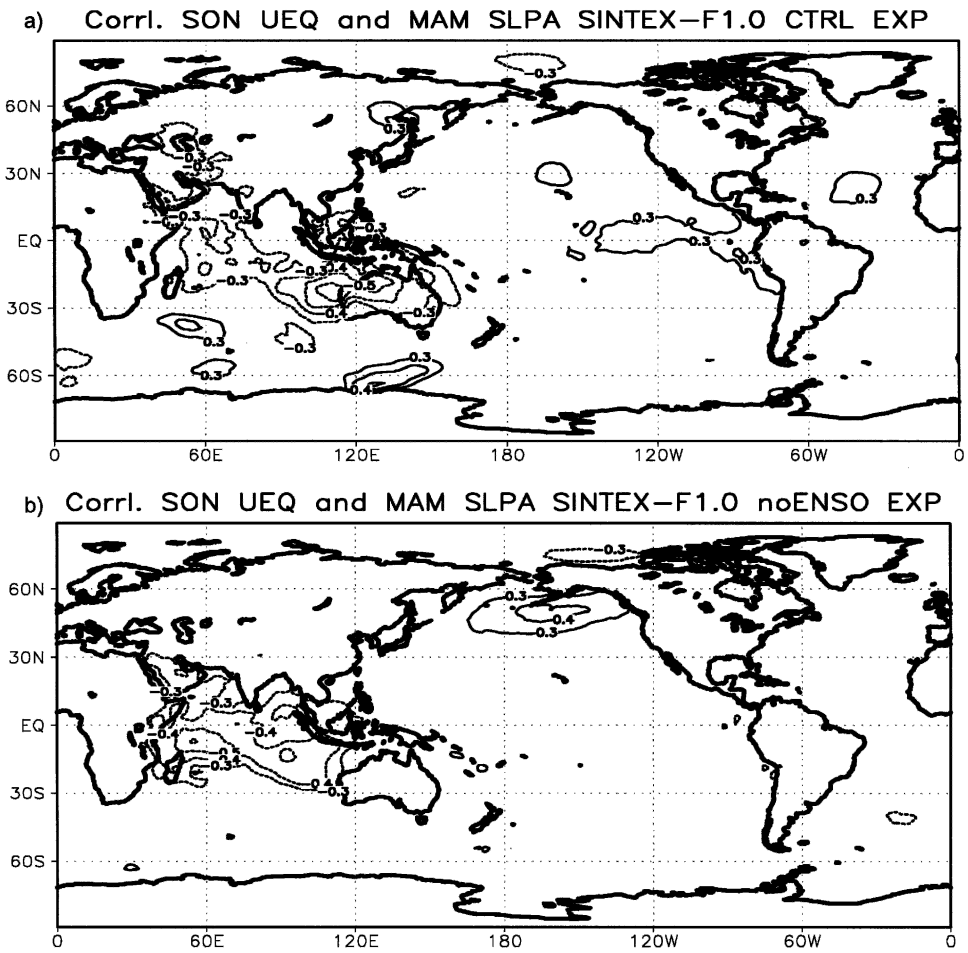

FIG. 14. Lag–correlation between ZWI and global sea level pressure anomalies for the (a) control experiment and (b) noENSO experiment. The ZWI of boreal fall lags the sea level pressure anomalies of boreal spring. Shown correlation coefficients are significant at the 99% of confidence level from a two-tailed Student's *t* test.

summer. In those cases, it is found that the anomalous tropospheric ascent in the central and western Pacific region is associated with subsidence over the western Indian Ocean in March–May (Fig. 15a). The associated lower-tropospheric divergence gives rise to westerlies in the eastern Indian Ocean (Fig. 16a). However, the descending region intensifies and shifts to the eastern Indian Ocean in boreal summer (Fig. 15b) when the Pacific ascending region moves eastward. This brings the lower-tropospheric anomalous high closer to the Indonesian coast. The associated strengthening of southeasterlies off Java then favors development of the IOD in summer (Fig. 16b) through coevolving ocean processes. The eastward movement of the model velocity potentials is consistent with the observational finding that zonal divergent wind anomalies propagate eastward from the Indian Ocean to the Pacific (Yasunari 1985; White and Cayan 2000), leading to a favorable precondition for warm phase of ENSO (Yamagata and Masumoto 1989).

In the 42% of cases in which unfavorable conditions in spring turned to favorable conditions in summer, we find that 70% (i.e., 29% of total IOD events) of IOD events are associated with the ENSO. This is also consistent with the observational finding that substantial numbers of concurrent IOD events develop after boreal spring (e.g., RAO).

Besides the atmospheric bridge that explains the ENSO influences on the IOD initiation, we also find a significant oceanic connection in the model results. In the control experiment, because of the bias to concurrent IODs, we notice that the correlation between ZWI and sea level pressure anomalies peaks near the west coast of Australia (Fig. 14a). These sea level anomalies are associated with significant cold SST anomalies as seen in the March–May composite (Fig. 16a). Associ-

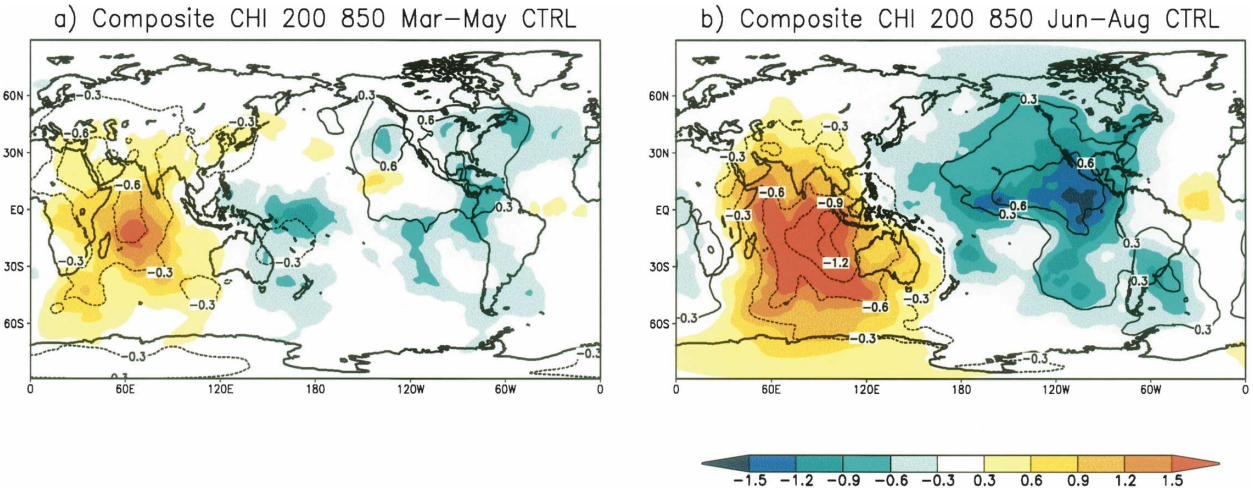

FIG. 15. Composites of velocity potential anomalies for those 42% of positive IOD events that develop in spite of March–May unfavorable wind conditions in the control experiment for (a) March–May and (b) June–August. Anomalies are scaled by a factor of 10^6. Anomalies from 200 (850) hPa are shaded (contoured). Shown values exceed the 90% level of statistical significance from a two-tailed Student's *t* test.

ated with the ENSO variability, the Pacific water enters into the eastern Indian Ocean and then propagates along the Australian coast (Clarke and Liu 1994; Meyers 1996), leading to local air–sea interaction (Hendon 2003). In one of the recent studies, Cai et al. (2005) have reported that almost all positive IOD events in their CGCM are initiated by the intrusion of the cold western Pacific water following warm ENSO events. In the present analysis, we did not find many such occurrences wherein decaying ENSO initiates the IOD through the variation of the Indonesian Throughflow. Because of wider Indonesian passages owing to low horizontal resolution, CGCM results of Cai et al. (2005) show excessive leakage of the western Pacific signal into the eastern Indian Ocean. The lack of the biennial signal in their model IOD variability may be attributed to this model bias.

The formation of IOD is suggested to be associated with yet another external factor in the Southern Hemisphere extratropics (Lau and Nath 2004). This signal marked by sea level perturbation south of Australia is shown to be related to the Southern Hemisphere annular mode/Antarctic Oscillation. In our control experiment, from the correlation between ZWI and sea

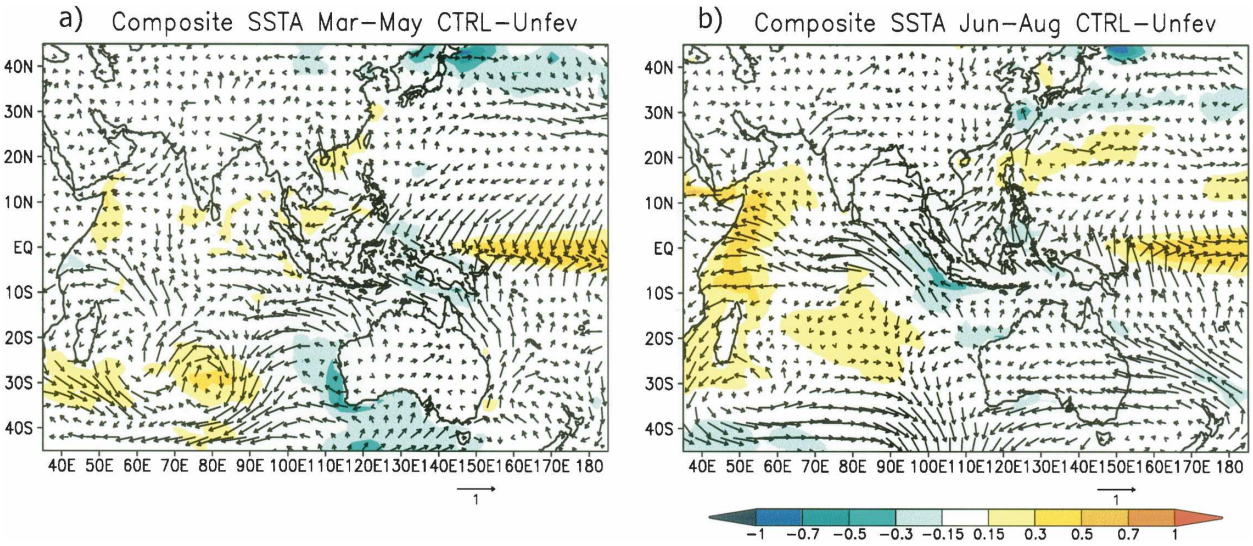

FIG. 16. Same as in Fig. 15, but for composites of SST and wind anomalies.

level pressure anomalies, we also notice a small regional correlation pattern located south of Australia (Fig. 14a). Contrary to the previous study, we did not find much evidence of a connection between this atmospheric perturbation and the Antarctic Oscillation in our results. However, we note that SINTEX-F1 does not include an ice model. This might have introduced model bias for proper representation of the Antarctic Oscillation. Nevertheless, most of the correlations seen south of Australia in our model results are simultaneous with the correlations in the southern tropical Indian Ocean. Therefore it is unlikely that the region south of Australia has a significant contribution to the IOD initiation in the present model results. Rather, the signal south of Australia may be due to atmospheric teleconnection excited by the tropical tropospheric divergences related to evolution of either IOD or ENSO.

5. Conclusions

It is found from the observation that only 30% of IOD events develop in conjunction with ENSO events (e.g., Rao et al. 2002; Yamagata et al. 2004). Nevertheless, several studies raised a doubt on the independent existence of IOD (Baquero-Bernal et al. 2002; Dommenget and Latif 2002; Hastenrath 2002). The present study employs SINTEX-F1 CGCM to examine the independent evolution of IOD by decoupling the tropical Pacific Ocean from atmosphere in a numerical experiment. A comparison of results between the noENSO experiment and the globally coupled model experiment shows the intrinsic nature of IOD and possible alterations by concurrent IODs.

The noENSO experiment demonstrates the independent existence of IOD and the associated coupled feedback processes in the tropical Indian Ocean in the absence of ENSO. The IOD takes a dominant seat in this model experiment by becoming the first EOF mode. This is consistent with previous statistical results obtained by linearly separating the ENSO effect in the observed data (Yamagata et al. 2003; Behera et al. 2003). In addition, it is found that the interannual IOD variability is dominantly biennial in the noENSO experiment. In comparison, dominant peaks for the interannual IOD in the control experiment and data are 3–4 and 4–6 yr, respectively. This suggests that the ENSO variability modifies the intrinsic IOD variability. We have found that the ENSO in the tropical Pacific influences the interannual frequency of IODs by modulating the latter's formation mechanism through the Walker circulation. This is examined by preparing conditional composites that consider the Indian Ocean condition during the coevolving IOD and ENSO events. It is found that 42% of spring unfavorable conditions for positive IOD events are turned into favorable conditions through the Pacific influences. The eastern intensification of lower-tropospheric divergence in relation to the anomalous ascending motions in the central Pacific gives rise to upwelling-favorable winds along the Java–Sumatra coast. This sets the ocean–atmosphere interaction and initiates a positive IOD in boreal summer. In contrast, pure IOD events unrelated to ENSO events form in boreal spring by intrinsic ocean–atmosphere processes.

The ENSO influence also is seen through the oceanic route. The western Pacific signal enters the Indian Ocean through the Indonesian passages and propagates along the coast of Western Australia. The cold anomalies transmitted from the western Pacific are concurrent with the anomalous high in the southern tropical Indian Ocean. The anomalous high, in turn, could give rise to favorable equatorial winds for the development of a positive IOD event.

These interactions of ENSO and IOD do not necessarily mean that the IODs are triggered by only external forcings arising from the coupled variabilities in the tropical Pacific. Similar to the observation, only about 29% of IOD events coevolve with ENSOs. Furthermore, we find that 58% of positive IOD events in the control experiment evolve from favorable equatorial wind anomalies internal to the Indian Ocean. This happens in 82% of the cases of positive IODs in the noENSO experiment: cold anomalies in the western tropical Indian Ocean during the boreal fall of the year previous to an IOD propagate to the Sumatra–Java coast to trigger an IOD event. Additionally, the western anomalies substantially affect ISD activities aiding the IOD formation further. Those early favorable conditions offer better scope for IOD predictability in case of independent IOD events as compared to those arising through interactions with ENSO. On the other hand, the western SST anomalies for pure IOD events are somewhat weaker as compared to that in concurrent IOD events. Weaker evaporation and vertical upper-ocean heat convergence, owing to ENSO-altered winds, in the western Indian Ocean lead to warmer SST anomalies for positive concurrent IOD events and vice versa. The predictability study of the IOD events is a real challenge, and its progress will also contribute to the ENSO forecast: we find that the ENSO variability changes in the absence of IOD in the noIOD experiment.

Acknowledgments. We thank Drs. Silvio Gualdi, Antonio Navarra, Guruvan Madec, and Pascale Delecluse for numerous interactions during the development of the SINTEX-F1. We are thankful to two anonymous

reviewers for their constructive remarks that helped to improve the content of the manuscript. We also thank Drs. Tomoki Tozuka, Yukio Masumoto, Karumuri Ashok, Gary Meyers, Mark Jury, Saji Hameed, and Reiko Suzuki for useful discussions.

REFERENCES

Annamalai, H., R. Murtugudde, J. Potemra, S. P. Xie, P. Liu, and B. Wang, 2003: Coupled dynamics over the Indian Ocean: Spring initiation of the Zonal Mode. *Deep-Sea Res.,* **50,** 2305–2330.

Ashok, K., W. Chan, T. Motoi, and T. Yamagata, 2004: Decadal variability of the Indian Ocean Dipole. *Geophys. Res. Lett.,* **31,** L24207, doi:10.1029/2004GL021345.

Baquero-Bernal, A., M. Latif, and S. Legutke, 2002: On dipole-like variability in the tropical Indian Ocean. *J. Climate,* **15,** 1358–1368.

Behera, S. K., and T. Yamagata, 2001: Subtropical SST dipole events in the southern Indian Ocean. *Geophys. Res. Lett.,* **28,** 327–330.

——, and ——, 2003: Influence of the Indian Ocean Dipole on the Southern Oscillation. *J. Meteor. Soc. Japan,* **81,** 169–177.

——, R. Krishnan, and T. Yamagata, 1999: Unusual ocean-atmosphere conditions in the tropical Indian Ocean during 1994. *Geophys. Res. Lett.,* **26,** 3001–3004.

——, P. S. Salvekar, and T. Yamagata, 2000: Simulation of interannual SST variability in the tropical Indian Ocean. *J. Climate,* **13,** 3487–3499.

——, S. A. Rao, H. N. Saji, and T. Yamagata, 2003: Comments on "A cautionary note on the interpretation of EOFs." *J. Climate,* **16,** 1087–1093.

——, J.-J. Luo, S. Masson, P. Delecluse, S. Gualdi, A. Navarra, and T. Yamagata, 2005: Paramount impact of the Indian Ocean dipole on the East African short rains: A CGCM study. *J. Climate,* **18,** 4514–4530.

Bjerknes, J., 1969: Atmospheric teleconnections from the equatorial Pacific. *Mon. Wea. Rev.,* **97,** 163–172.

Cai, W., H. Hendon, and G. Meyers, 2005: Indian Ocean dipole-like variability in the CSIRO Mark 3 coupled climate model. *J. Climate,* **18,** 1449–1468.

Carton, J., G. Chepurin, X. Cao, and B. Giese, 2000: A simple ocean data assimilation analysis of the global upper ocean 1950–95. Part I: Methodology. *J. Phys. Oceanogr.,* **30,** 294–309.

Clarke, A. J., and X. Liu, 1994: Interannual sea level in the northern and eastern Indian Ocean. *J. Phys. Oceanogr.,* **24,** 1224–1235.

Dommenget, D., and M. Latif, 2002: A cautionary note on the interpretation of EOFs. *J. Climate,* **15,** 216–225.

Feng, M., and G. Meyers, 2003: Interannual variability in the tropical Indian Ocean: A two-year time scale of IOD. *Deep-Sea Res.,* **50B,** 2263–2284.

Gualdi, S., E. Guilyardi, A. Navarra, S. Masina, and P. Delecluse, 2003: The interannual variability in the tropical Indian Ocean as simulated by a CGCM. *Climate Dyn.,* **20,** 567–582.

Guilyardi, E., P. Delecluse, S. Gualdi, and A. Navarra, 2001: The role of lateral ocean physics in the upper ocean thermal balance of a coupled ocean-atmosphere GCM. *Climate Dyn.,* **17,** 589–599.

Hastenrath, S., 2002: Dipoles, temperature gradient, and tropical climate anomalies. *Bull. Amer. Meteor. Soc.,* **83,** 735–738.

——, and D. Polzin, 2004: Dynamics of the surface wind field over the equatorial Indian Ocean. *Quart. J. Roy. Meteor. Soc.,* **130,** 503–517.

——, A. Nicklis, and L. Greischar, 1993: Atmospheric-hydrospheric mechanisms of climate anomalies in the western equatorial Indian Ocean. *J. Geophys. Res.,* **98** (C11), 20 219–20 235.

Hendon, H. H., 2003: Indonesian rainfall variability: Impacts of ENSO and local air–sea interaction. *J. Climate,* **16,** 1775–1790.

Huang, B., and J. L. Kinter III, 2002: The interannual variability in the tropical Indian Ocean. *J. Geophys. Res.,* **107,** 3199, doi:10:1029/2001JC001278.

Iizuka, S., T. Matsuura, and T. Yamagata, 2000: The Indian Ocean SST dipole simulated in a coupled general circulation model. *Geophys. Res. Lett.,* **27,** 3369–3372.

Jury, R. M., and B. Huang, 2004: The Rossby wave as a key mechanism of Indian Ocean climate variability. *Deep-Sea Res.,* **51,** 2123–2136.

Kawamura, R., 1994: A rotated EOF analysis of global sea surface temperature variability with interannual and decadal scales. *J. Phys. Oceanogr.,* **24,** 707–715.

Klein, S. A., B. J. Soden, and N.-C. Lau, 1999: Remote sea surface temperature variations during ENSO: Evidence for a tropical atmospheric bridge. *J. Climate,* **12,** 917–932.

Lau, N.-C., and M. J. Nath, 2004: Coupled GCM simulation of atmosphere–ocean variability associated with zonally asymmetric SST changes in the tropical Indian Ocean. *J. Climate,* **17,** 245–265.

Li, T., B. Wang, C. P. Chang, and Y. Zhang, 2003: A theory for the Indian Ocean dipole–zonal mode. *J. Atmos. Sci.,* **60,** 2119–2135.

Luo, J. J., S. Masson, S. Behera, P. Delecluse, S. Gualdi, A. Navarra, and T. Yamagata, 2003: South Pacific origin of the decadal ENSO-like variations as simulated by a coupled GCM. *Geophys. Res. Lett.,* **30,** 2250, doi:10.1029/2003GL018649.

——, ——, ——, S. Shingu, and T. Yamagata, 2005a: Seasonal climate predictability in a coupled OAGCM using a different approach for ensemble forecasts. *J. Climate,* **18,** 4474–4497.

——, ——, E. Roeckner, G. Madec, and T. Yamagata, 2005b: Reducing climatology bias in an ocean–atmosphere CGCM with improved coupling physics. *J. Climate,* **18,** 2344–2360.

Madec, G., P. Delecluse, M. Imbard, and C. Levy, 1998: OPA version 8.1 ocean general circulation model reference manual. Tech. Rep./Note 11, LODYC/IPSL, Paris, France, 91 pp.

Masson, S., and Coauthors, 2005: Impact of barrier layer on winter-spring variability of the southeastern Arabian Sea. *Geophys. Res. Lett.,* **32,** L07703, doi:10.1029/2004GL021980.

McCreary, J. P., P. K. Kundu, and R. Molinari, 1993: A numerical investigation of dynamics, thermodynamics and mixed-layer processes in the Indian Ocean. *Progress in Oceanography,* Vol. 31, Pergamon, 181–244.

Meyers, G., 1996: Variation of Indonesian throughflow and El Niño-Southern Oscillation. *J. Geophys. Res.,* **101,** 12 255–12 263.

Murtugudde, R., and A. J. Busalacchi, 1999: Interannual variability in the dynamics and thermodynamics of the tropical Indian Ocean. *J. Climate,* **12,** 2300–2326.

Pan, Y.-H., and A. Oort, 1990: Correlation analyses between sea surface temperature anomalies in the eastern equatorial Pacific and the world ocean. *Climate Dyn.,* **4,** 191–205.

Rao, S. A., and T. Yamagata, 2004: Abrupt termination of Indian Ocean dipole events in response to intraseasonal disturbances. *Geophys. Res. Lett.,* **31,** L19306, doi:10.1029/2004GL020842.

——, and S. K. Behera, 2005: Subsurface influence on SST in the tropical Indian Ocean structure and interannual variabilities. *Dyn. Atmos. Oceans,* **39,** 103–135.

——, ——, Y. Masumoto, and T. Yamagata, 2002: Interannual variability in the subsurface tropical Indian Ocean with a special emphasis on the Indian Ocean Dipole. *Deep-Sea Res.,* **49B,** 1549–1572.

Rayner, N. A., D. E. Parker, E. B. Horton, C. K. Folland, L. V. Alexander, D. P. Rowell, E. C. Kent, and A. Kaplan, 2003: Global analyses of sea surface temperature, sea ice, and night marine air temperature since the late nineteenth century. *J. Geophys. Res.,* **108,** 4407, doi:10.1029/2002JD002670.

Roeckner, E., and Coauthors, 1996: The atmospheric general circulation model ECHAM4: Model description and simulation of present day climate. Max-Plank-Institut fur Meteorologie Rep. 218, Hamburg, Germany, 90 pp.

Saji, N. H., and T. Yamagata, 2003: Interference of teleconnection patterns generated from the tropical Indian and Pacific Oceans. *Climate Res.,* **25,** 151–169.

——, B. N. Goswami, P. N. Vinayachandran, and T. Yamagata, 1999: A dipole mode in the tropical Indian Ocean. *Nature,* **401,** 360–363.

Shinoda, T., M. A. Alexander, and H. H. Hendon, 2004: Remote response of the Indian Ocean to interannual SST variations in the tropical Pacific. *J. Climate,* **17,** 362–372.

Suzuki, R., S. K. Behera, S. Iizuka, and T. Yamagata, 2004a: The Indian Ocean subtropical dipole simulated using a CGCM. *J. Geophys. Res.,* **109,** C09001, doi:10.1029/2003JC001974.

Tourre, Y. M., and W. B. White, 1995: ENSO signals in global upper-ocean temperature. *J. Phys. Oceangr.,* **25,** 1317–1332.

Tozuka, T., J.-J. Luo, S. Masson, S. K. Behera, and T. Yamagata, 2005: Annual ENSO simulated in a coupled ocean-atmosphere model. *Dyn. Atmos. Oceans,* **39,** 41–60.

——, ——, ——, and T. Yamagata, 2006: Decadal Indian Ocean dipole simulated in an ocean–atmosphere coupled model. *J. Climate,* in press.

Valcke, S., L. Terray, and A. Piacentini, 2000: The OASIS coupler user guide version 2.4. Tech. Rep. TR/CMGC/00-10, CERFACS, Toulouse, France, 85 pp.

Venzke, S., M. Latif, and A. Villwock, 2000: The coupled GCM ECHO-2. Part II: Indian Ocean response to ENSO. *J. Climate,* **13,** 1371–1383.

Vinayachandran, P. N., N. H. Saji, and T. Yamagata, 1999: Response of the equatorial Indian Ocean to an anomalous wind event during 1994. *Geophys. Res. Lett.,* **26,** 1613–1616.

Wajsowicz, R. C., 2005: Forecasting extreme events in the tropical Indian Ocean sector climate. *Dyn. Atmos. Oceans,* **39,** 137–151.

Webster, P. J., A. Moore, J. Loschnigg, and M. Leban, 1999: Coupled ocean–atmosphere dynamics in the Indian Ocean during 1997–98. *Nature,* **401,** 356–360.

White, W. B., and D. R. Cayan, 2000: A global El Niño–Southern Oscillation wave in surface temperature and pressure and its interdecadal modulation from 1900 to 1997. *J. Geophys. Res.,* **105,** 11 232–11 242.

Xie, S.-P., H. Annamalai, F. Schott, and J. P. McCreary, 2002: Structure and mechanisms of South Indian Ocean climate variability. *J. Climate,* **15,** 864–878.

Yamagata, T., and Y. Masumoto, 1989: A simple ocean-atmosphere coupled model for the origin of a warm El Niño Southern Oscillation event. *Philos. Trans. Roy. Soc. London,* **329,** 225–236.

——, S. K. Behera, S. A. Rao, Z. Guan, K. Ashok, and H. N. Saji, 2003: Comments on "Dipoles, temperature gradient, and tropical climate anomalies." *Bull. Amer. Meteor. Soc.,* **84,** 1418–1422.

——, ——, J.-J. Luo, S. Masson, M. Jury, and S. A. Rao, 2004: Coupled ocean-atmosphere variability in the tropical Indian Ocean. *Earth Climate: The Ocean-Atmosphere Interaction, Geophys. Monogr.,* No. 147, Amer. Geophys. Union, 189–212.

Yasunari, T., 1985: Zonally propagating modes of the global east-west circulation associated with the Southern Oscillation. *J. Meteor. Soc. Japan,* **63,** 1013–1029.

Yu, J.-Y., and K. M. Lau, 2004: Contrasting Indian Ocean SST variability with and without ENSO influence: A coupled atmosphere-ocean GCM study. *Meteor. Atmos. Phys.,* **90,** doi:10.1007/s00703-004-0094-7.